



PCCP

**Strain tuning high thermal conductivity in Boron Phosphide  
at nanometer length scales– A first-principles study**

Journal:	<i>Physical Chemistry Chemical Physics</i>
Manuscript ID	CP-COM-07-2020-003690.R1
Article Type:	Paper
Date Submitted by the Author:	10-Aug-2020
Complete List of Authors:	Muthaiah, Rajmohan; University of Oklahoma, School of Aerospace and Mechanical Engineering Garg, Jivtesh; University of Oklahoma, School of Aerospace and Mechanical Engineering

SCHOLARONE™  
Manuscripts

## Strain tuning high thermal conductivity in Boron Phosphide at nanometer length scales– A first-principles study

Rajmohan Muthaiah and Jivtesh Garg

School of Aerospace and Mechanical Engineering, University of Oklahoma, Norman, OK  
73019, USA.

### Abstract:

Breakdown of Fourier law of heat conduction at nanometer length scales significantly diminishes thermal conductivity, leading to challenges in thermal management of nanoelectronics applications. In this work we demonstrate using first-principles computations that biaxial strain can enhance  $k$  at nanoscale in Boron Phosphide (BP), yielding nanoscale  $k$  values that exceed even the bulk  $k$  value of silicon. At length scale of  $L = 200$  nm,  $k$  of 4% biaxially strained BP, is enhanced by 25% to a value of 150.4 W/mK, relative to 120 W/mK computed for unstrained BP at 300 K. Enhancement in  $k$  at nanoscale is found to be due to suppression of anharmonic scattering in the higher frequency range where phonon meanfreepaths are in nanometers, mediated by an increase in phonon band gap in strained BP. Such suppression in scattering enhances meanfreeapths in the nanometer regime, thus enhancing nanoscale  $k$ . First-principles computations based on deriving harmonic and anharmonic force interactions from density-functional theory are used to provide detailed understanding of the effect in terms of individual scattering channels.

Keywords: High thermal conductivity, first-principles calculations, boron phosphide, biaxial strain, anharmonic phonon scattering

### Introduction:

As system length scale diminishes to nanometers, phonon scattering at boundaries becomes pronounced, dramatically decreasing effective thermal conductivity ( $k$ ) below the bulk value (Fourier limit)<sup>1</sup>. This diminished heat transfer at nanoscale can lead to overheating and a decrease in reliability and performance in nanoelectronic applications<sup>1, 2</sup>. Size-dependent decrease in thermal conductivity has been reported experimentally in both bulk and nano materials<sup>3-6</sup>. To improve heat dissipation at nanoscale, there is a strong need for materials with enhanced thermal conductivity at these length scales. In this work, we show using first-principles computations, that biaxial strain can significantly enhance thermal conductivity of Boron Phosphide at nanoscale, yielding nanoscale  $k$  values that even exceed the bulk  $k$  value of silicon. These results have important implications for thermal management of nanoelectronics.

Materials like Boron-Phosphide (BP) have a large phonon band gap in their vibration spectra due to large mismatch in masses of the constituent atoms. In recent years, such a phonon gap has been shown to suppress scattering of acoustic phonons by optical phonons, enhancing phonon lifetimes, and thus thermal conductivity<sup>7-13</sup> in a wide range of materials. In particular, the effect was shown to lead to a thermal conductivity approaching  $\sim 1000$  W/mK in Boron Arsenide (BAs)<sup>7, 10, 12, 14</sup>. The effect can be understood by observing that anharmonic scattering of phonons through the lowest-order three phonon processes can

be classified into two categories - absorption scattering process, where a phonon mode ( $q\omega$ ) scatters by absorbing another phonon mode ( $q'\omega'$ ), yielding a higher energy ( $q''\omega''$ ) phonon mode, and decay processes, where a phonon mode decays into two lower energy phonons. These processes satisfy energy and momentum conservation given by,  $\omega + \omega' = \omega''$  (energy),  $q + q' = q''$  (momentum) for absorption process and  $\omega = \omega' + \omega''$  (energy),  $q = q' + q''$  (momentum) for decay process. Fig. 1 shows that in Silicon, an acoustic phonon ( $q\omega$ ) can scatter by absorbing another acoustic phonon ( $q'\omega'$ ) to yield an optical phonon ( $q''\omega''$ ), satisfying both momentum and energy conservation. However, in Boron-Arsenide (BAs), the large phonon gap implies that the third phonon required for energy conservation, does not exist, forbidding this scattering process. Such a suppression of scattering of acoustic phonons dramatically enhances lifetimes and thermal conductivity. BP was recently demonstrated to exhibit high bulk  $k$  in the range of  $\sim 600$  W/mK<sup>12, 15-17</sup>.

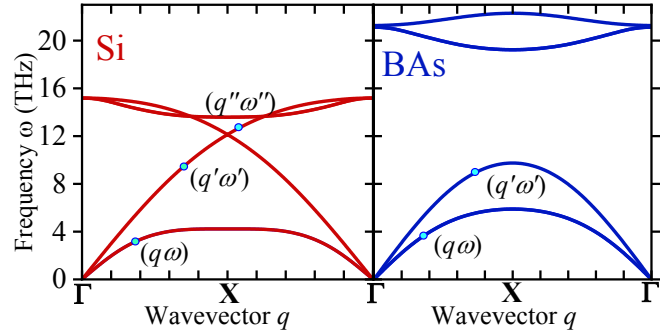


Figure 1: Phonon dispersions of Silicon and Boron-Arsenide showing effect of phonon band gap on suppressing anharmonic scattering of acoustic phonons.

Strain can further enhance  $k$  by increasing phonon band gap, thus further suppressing scattering of acoustic phonons leading to even higher phonon lifetimes. Lindsay *et al.*<sup>17</sup> demonstrated the effect of isotropic strain on bulk  $k$  enhancement through first-principles computations. Compressive strain was revealed to suppress above presented scattering channel in materials like Magnesium Oxide (MgO) and Silicon Carbide (SiC), enhancing their bulk  $k$ .

While above work addressed bulk  $k$ , in this work we demonstrate that in materials with a phononic band gap, strain can specifically enhance  $k$  at nanoscale. To understand this, it should be noted that  $k$  contribution of a phonon mode is proportional to its meanfreepath,  $\Lambda$  ( $k \propto \Lambda$ ). Meanfreepaths typically decrease with increase in frequency, being in microns at lower frequencies, and decreasing to nanometer values as frequencies increase. Strain suppresses anharmonic scattering of phonons at frequencies larger than the magnitude of phonon band gap ( $\sim$ high frequencies). At these frequencies, phonon meanfreepaths are potentially in the nanometer range; suppression of scattering thus enhances  $\Lambda$  in the nanometer range, directly contributing to  $k$  enhancement at nanoscale. Outlined effect, demonstrated in this work, can lead to novel pathways for improving thermal management at nanometer length scales in a wide range of applications. We demonstrate the effect in BP using first-principles approach outlined below. We first describe the first-principles approach, followed by thermal conductivity results and analysis.

The first-principles approach<sup>18-21</sup> for predicting thermal conductivity involves exactly solving the phonon Boltzmann transport equation (PBTE)<sup>18</sup>. The most important ingredients, namely the 2<sup>nd</sup> and 3<sup>rd</sup> order interatomic force constants (IFCs), needed for  $k$  prediction, are derived from density-functional theory (DFT)<sup>22, 23</sup>. DFT has been shown to yield highly accurate IFCs, overcoming limitations of empirical potentials, leading to unprecedented accuracy<sup>20</sup> in the prediction of lattice  $k$ . For analysis and discussion, it is useful to present the expression for thermal conductivity ( $k$ ), predicted based on solving PBTE<sup>21</sup> in the single mode relaxation time (SMRT) approximation, as given below<sup>24</sup> (typically providing good estimate of  $k$ ),

$$k_\alpha = \frac{\hbar^2}{N\Omega k_b T^2} \sum_\lambda v_{\alpha\lambda}^2 \omega_\lambda^2 \bar{n}_\lambda (\bar{n}_\lambda + 1) \tau_\lambda \quad (1)$$

where  $\alpha$ ,  $\hbar$ ,  $\Omega$ ,  $k_b$ ,  $T$ , are the cartesian direction, Planck constant, unit cell volume, Boltzmann constant, and absolute temperature respectively.  $\lambda$  represents the vibrational mode ( $\mathbf{q}j$ ) ( $\mathbf{q}$  is the wave vector and  $j$  represents phonon polarization).  $N$  is the size of the  $\mathbf{q}$  mesh used for summation in above equation.  $\omega_\lambda$ ,  $\bar{n}_\lambda$ , and  $v_{\alpha\lambda}$  ( $= \partial\omega_\lambda/\partial q$ ) are the phonon frequency, equilibrium Bose-Einstein population and group velocity along cartesian direction  $\alpha$ , respectively of a phonon mode  $\lambda$ . These are derived from the knowledge of phonon dispersion computed using 2<sup>nd</sup> order IFCs.  $\tau_\lambda$  is the phonon lifetime (equal to the inverse of scattering rate). In the SMRT approximation, phonon lifetime ( $\tau_\lambda$ ) of a vibrational mode  $\lambda$  is computed using the following equation,

$$\frac{1}{\tau_\lambda} = \pi \sum_{\lambda'\lambda''} |V_3(-\lambda, \lambda', \lambda'')|^2 \times [2(n_{\lambda'} - n_{\lambda''})\delta(\omega(\lambda) + \omega(\lambda') - \omega(\lambda'')) + (1 + n_{\lambda'} + n_{\lambda''})\delta(\omega(\lambda) - \omega(\lambda') - \omega(\lambda''))] \quad (2)$$

where  $V_3(-\lambda, \lambda', \lambda'')$  are the three-phonon coupling matrix elements. The first delta function in the above equation represents absorption scattering process and second delta function represents a decay process.

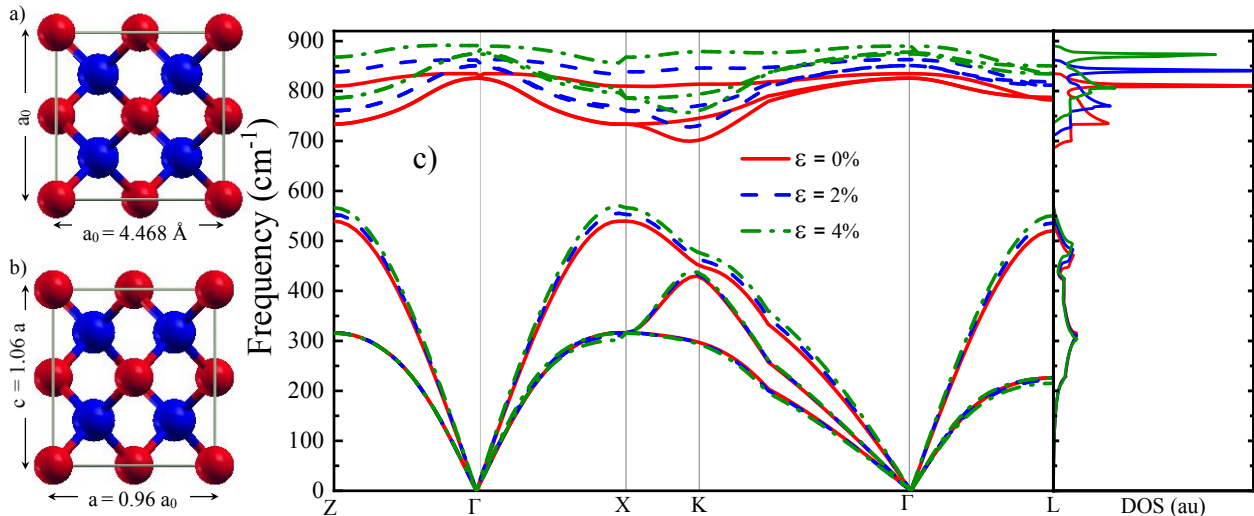


Figure 2: Cubic Boron-Phosphide with a) zero strain and b) biaxial strain of 4%, c) Phonon dispersion and density of states for the 0%, 2% and 4% biaxially strained BP.

DFT calculations were carried out using QUANTUM-ESPRESSO<sup>25</sup>. Norm-conserving pseudopotentials in the local-density approximation (LDA) were used with a plane-wave cut-off

of 100 Ry. Monkhorst<sup>26</sup>  $k$ -point mesh of  $12 \times 12 \times 12$  was used to describe the electronic properties.  $8 \times 8 \times 8$   $q$ -grid was used to compute dynamical matrices and the 2<sup>nd</sup> order IFCs. 3<sup>rd</sup> order IFCs were computed using D3Q<sup>18, 19, 27</sup> package, on a  $4 \times 4 \times 4$  supercell. Acoustic sum rules were imposed on both 2<sup>nd</sup> and 3<sup>rd</sup> order force constants. Phonon linewidth and  $k$  calculations were carried out on  $30 \times 30 \times 30$   $q$ -mesh. For the exact solution of PBTE, typically 10 iterations were found to be sufficient to achieve convergence<sup>18</sup>.

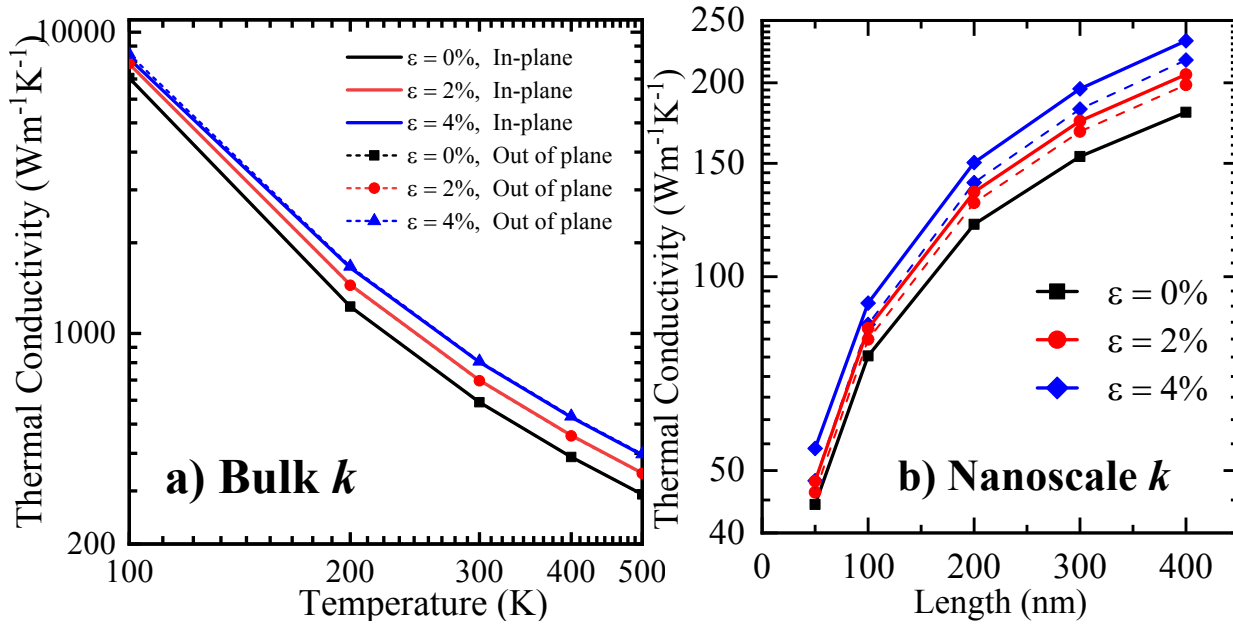


Figure 3: a) Computed thermal conductivity of 0%, 2% and 4% biaxially strained BP obtained by exactly solving PBTE, b) Enhancement in  $k$  at nanometer length scales in strained BP at 300 K. Dashed lines represent in-plane (plane in which biaxial compression is applied)  $k$ , while solid lines represent out-of-plane  $k$ .

Lattice parameter of unstrained BP was determined through energy minimization to be  $a_0 = 4.468$  Å. Computed phonon dispersion (in good agreement with the experimental measurements<sup>28</sup>) for unstrained case is shown in Fig. 2c. For the strained cases, the lattice was compressed by 2% and 4% in the  $x$ - $y$  plane (along both  $x$  and  $y$  directions) and relaxed in the  $z$ -direction (Fig. 2b). The lattice dimensions obtained after relaxing the structure corresponded to a Poisson ratio of 0.19, in good agreement with reported values<sup>29</sup>.

As the lattice is biaxially compressed, phonon band gap between acoustic and optical phonons increases from  $148$  cm<sup>-1</sup> for unstrained case to  $157$  cm<sup>-1</sup> and  $168.0$  cm<sup>-1</sup> for 2% and 4% compressive strains, respectively (Fig. 2c). This increase in band gap increases  $k$  (Fig. 3a). At 300K, while in-plane (defined as the plane in which compressive biaxial strain is applied)  $k$  of unstrained BP is computed to be  $591$  W/mK, for 2% and 4% strained BP, in-plane  $k$  is found to be enhanced to values of  $699$  W/mK and  $802.5$  W/mK (Fig. 3a), representing an increase of 18.3% and 35.8%, respectively, over unstrained BP (anisotropy in bulk  $k$  is found to be small). The value of  $802.5$  W/mK obtained for 4% strained BP is almost 5-times the  $k$  of silicon<sup>20</sup> ( $k = 155$  W/mK at 300K), providing avenues to significantly enhance heat dissipation in nanoelectronic applications. Fig. 3b shows that  $k$  is significantly enhanced at nanoscale. At  $L=200$  nm, an increase in out-of-plane  $k$  of 25% is observed at 300 K (Fig. 3b), from  $120.6$  W/mK, for strain,  $\epsilon=0\%$ , to  $150.4$

W/mK, for  $\varepsilon = 4\%$ . This enhanced value at  $\varepsilon = 4\%$  is almost equal to the bulk  $k$  value of silicon<sup>20</sup>. At 400 nm, the increase in  $k$  is even higher, by almost 30%, from 180 W/mK to 232.5 W/mK, for the same increase in strain (Fig. 3b). These large increases in nanoscale  $k$  point to the potential of applying biaxial strain for enhancement of nanoscale heat dissipation in electronic applications ( $k$  values at nanometer length scales were achieved by introducing additional Casimir scattering<sup>30</sup>,  $1/\tau_{boundary} = |\mathbf{v}|/L$ , where  $v$  is the phonon velocity, and  $L$  is system size, in the solution of PBTE).

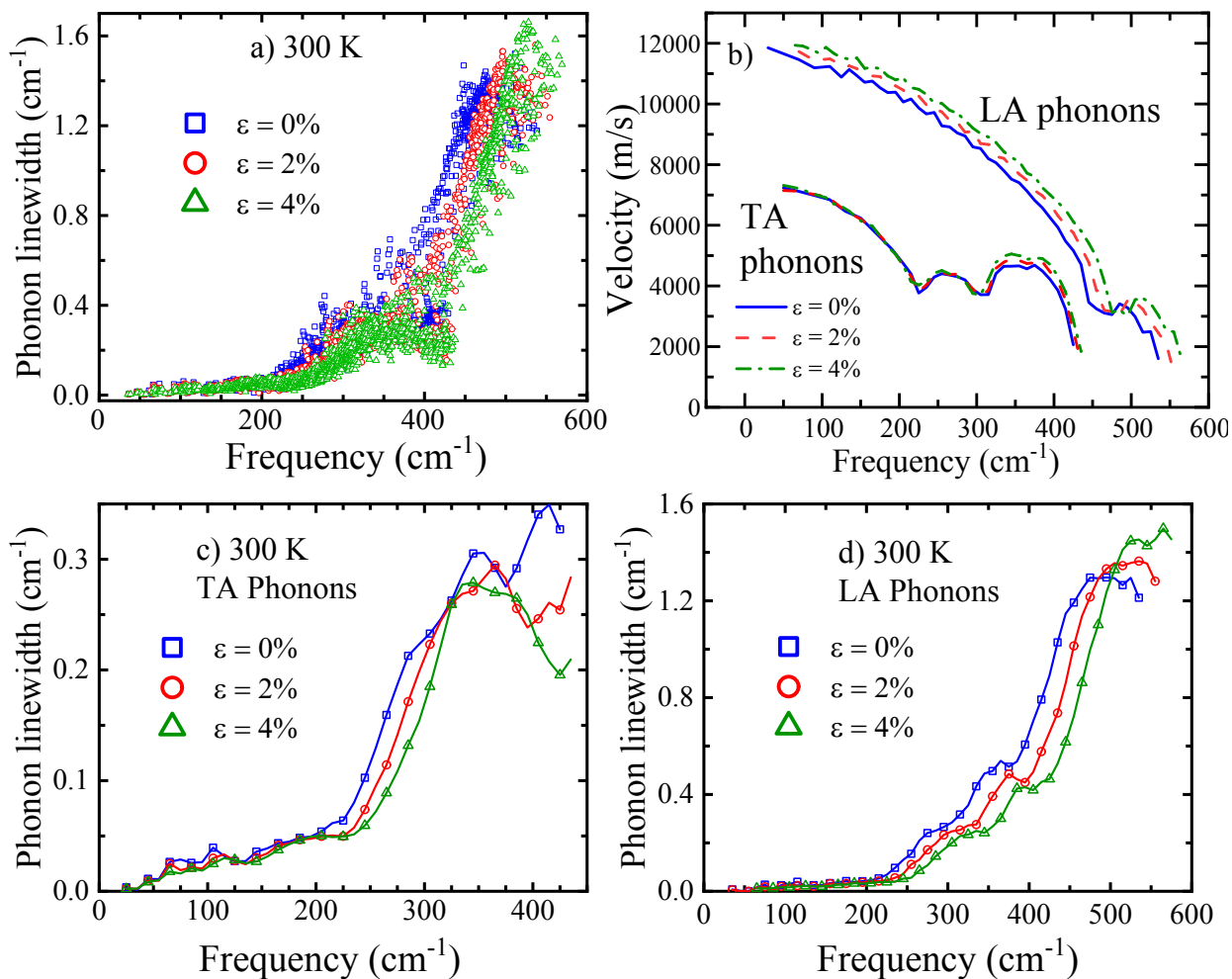


Figure 4: a) Comparison of phonon linewidths in unstrained and strained BP at 300 K, b) Mean phonon velocities at different frequencies for LA and TA phonons at different strains. Comparison of mean linewidths of c) TA phonons and d) LA phonons in unstrained and strained BP at 300 K.

We first describe increase in bulk  $k$  (seen in Fig. 3a) by comparing phonon scattering rates and group velocities of longitudinal acoustic (LA) and transverse acoustic (TA) phonons for unstrained and strained BP in Fig. 4 (ignoring optical phonons which are found to contribute less than 0.5% to overall  $k$ ). Strain significantly decreases scattering rates (Fig. 4a) and increases group velocities (Fig. 4b) of acoustic phonons. At a frequency of  $\sim 250$  cm<sup>-1</sup>, mean phonon linewidth of TA and LA modes in 4% strained BP is lower by 42% and 60%, relative to 0% strain case at 300 K (Figs. 4c and d). Significant increase in group velocities in strained BP is also visible in Fig.

4b, particularly for the LA phonons. These effects - decrease in scattering and increase in group velocities, together enhance bulk  $k$ . To approximately separate the effect of two on  $k$  enhancement, we recomputed  $k$  for hypothetical 4% strain case by imposing the linewidths to be the same as 0% case (but using the real velocities of 4% case). This resulted in a  $k$ , higher by only 12.8%, relative to 0% case, suggesting that decrease in phonon scattering rates (seen in Figs. 4a, c and d) is the dominant effect contributing to the observed 36%  $k$  enhancement in 4% strained BP.

Strain enhanced phonon band gap (Fig. 2c) leads to the above decrease in phonon scattering rates in biaxially compressed BP, as described next. Figs. 5a and b show that linewidths of both LA and TA modes decrease with increasing strain along  $\Gamma$ -X. In Figs. 5c and d, we investigate the following four scattering channels in scattering of LA and TA phonons - a)  $a + a \rightarrow o$ , b)  $a + o \rightarrow o$ , c)  $a + a \rightarrow a$ , and d)  $a \rightarrow a + a$  (a channel such as  $a + a \rightarrow o$  represents scattering of an acoustic phonon by absorbing another acoustic phonon yielding an optical phonon, whereas a channel such as  $a \rightarrow a + a$  represents decay of an acoustic phonon into two lower frequency acoustic phonons). For large part of  $\Gamma$ -X, the most significant contribution to scattering of LA and TA phonons in BP is from the  $a + a \rightarrow o$  scattering channel (Figs. 5c and d). At zone edge (point X),  $a + a \rightarrow o$  channel contributes 97.5% and 85.2% to total scattering rate of TA (Fig. 5d) and LA (Fig. 5c) modes, respectively.

Strain leads to a large decrease in magnitude of this dominant  $a + a \rightarrow o$  channel for TA mode along  $\Gamma$ -X direction (Fig. 5f). The role of strain mediated larger phonon band gap in decreasing  $a + a \rightarrow o$  scattering in strained BP (Fig. 5f) can be seen through an example, by considering that in unstrained case, a TA phonon of frequency  $\omega = 148 \text{ cm}^{-1}$  can scatter by absorbing an LA phonon of frequency  $\omega' = 540 \text{ cm}^{-1}$ , yielding the lowest energy optical phonon of frequency  $\omega'' = 688 \text{ cm}^{-1}$ , thus satisfying energy conservation,  $\omega + \omega' = \omega''$  (provided the momentum conservation is satisfied) (Fig. 2c). In the 2% strained case, however, due to the increase in phonon band gap, this scattering channel becomes forbidden, since the optical phonon frequencies are higher than  $688 \text{ cm}^{-1}$  (Fig. 2c), thus violating energy conservation. This dramatically suppresses phonon scattering through  $a + a \rightarrow o$  channel in strained BP. At Brillouin zone edge (X-point), for example, strain leads to a decrease in strength of this channel for TA modes by 16.1% and 28% for 2% and 4% strain, respectively, relative to 0% strain (Fig. 5f). For LA phonon mode (Fig. 5e),  $a + a \rightarrow o$  scattering again decreases for most part of  $\Gamma$ -X, except close to the Brillouin zone edge (near X) (cause of increase in  $a + a \rightarrow o$  scattering for LA modes in a small region near zone edge, as well as comparison of scattering channels for the entire Brillouin zone, are presented in supporting information). This decrease in scattering increases heat conduction by LA and TA phonons in strained BP. Overall, while LA and TA phonons contribute 137.0 W/mK and 399.3 W/mK to total  $k$  in unstrained BP at 300 K, their heat conduction increases by 20.3% and 17.6%, respectively in 2% strained BP and by 41.8% and 33.8%, respectively, in 4% strained BP, relative to the 0% strain case.

Nanoscale  $k$  enhancement (Fig. 3b) can now be understood by observing that strain mediated decrease in  $a + a \rightarrow o$  scattering is particularly dominant at higher frequencies exceeding  $200 \text{ cm}^{-1}$  (Fig. 4a, c and d) and higher wavevectors (Figs. 5e and f), as described next. At small wavevectors, the frequencies of acoustic phonons are too small to allow scattering into higher frequency optical phonons through the  $a + a \rightarrow o$  channel, causing contribution of  $a + a \rightarrow o$  channel to overall scattering to be weak. Note that  $a + a \rightarrow o$  scattering is completely forbidden in unstrained BP below frequencies of  $148 \text{ cm}^{-1}$ , equal to the phonon band gap, since a minimum of

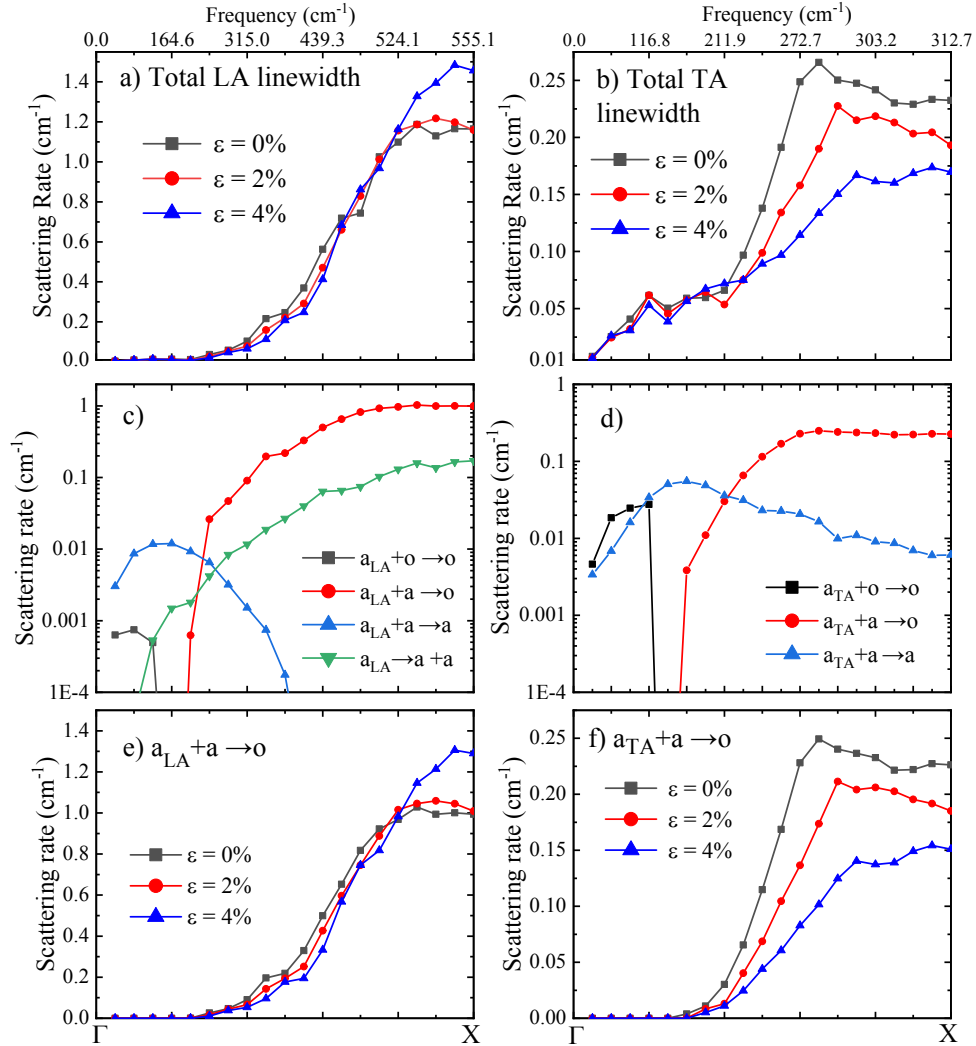


Figure 5: a) Comparison of total phonon linewidth of phonons along  $\Gamma$ -X in unstrained and strained BP at 300 K for a) LA (longitudinal acoustic) and TA (transverse acoustic) modes. Contribution of dominant scattering channels at 300 K to total scattering rate in unstrained BP for c) LA and d) TA modes. Comparison of scattering at 300 K due to e) and f)  $a + a \rightarrow o$  channel. The top scale represents average of the frequencies of LA and TA phonons in 0%, 2% and 4% strained BP along  $\Gamma$ -X.

148  $\text{cm}^{-1}$  is needed to absorb another acoustic phonon to reach the lowest frequency optical phonon,  $\omega_{min}^{acoustic}(148 \text{ cm}^{-1}) + \omega_{max}^{acoustic}(540 \text{ cm}^{-1}) = \omega_{min}^{optical}(688 \text{ cm}^{-1})$ . An increase in frequency, makes the energy conservation for  $a + a \rightarrow o$  channel progressively more feasible, causing the contribution of this channel to increase at higher frequencies. Increase in phononic band gap in strained BP, now by suppressing this large  $a + a \rightarrow o$  channel contribution to scattering at higher frequencies (Figs. 4e and f), thus also facilitates large decrease in overall scattering rates at higher frequencies  $> 200 \text{ cm}^{-1}$  (Fig. 4a). This effect is also seen to manifest as an increase in spectral contribution to  $k$  from higher frequency phonons in strained BP (Fig. 6c). In 4% strained BP, for example, phonon of frequencies  $> 200 \text{ cm}^{-1}$ , contribute 445.1 W/mK (55.5%) to overall  $k$ , significantly higher relative to unstrained BP, where corresponding phonons only contribute 278.9 W/mK (47.2%).

Enhancement in nanoscale  $k$  is directly related to above increase in thermal transport at higher frequencies. Phonon meanfreepaths ( $\Lambda_\lambda = \tau_\lambda v_\lambda$ ) generally decrease with increase in frequency due to increase in scattering, being in micron range at lower frequencies  $< 100 \text{ cm}^{-1}$  in BP (see Figs. 6a and b). At higher frequencies  $> 200 \text{ cm}^{-1}$  (where  $a + a \rightarrow o$  channel is active), Figs. 6a and b show that  $\Lambda$  in unstrained BP are mostly in the nanometer range ( $\Lambda$  for TA phonons are seen to be below 600 nm) and contribute strongly to  $k$  at nanoscale lengths. A decrease in  $a + a \rightarrow o$  scattering at these higher frequencies then enhances both TA and LA phonon meanfreepaths in the nanometer regime (Fig. 6a and b).

$k$  at any length scale  $L$  is primarily an aggregate of heat conduction by phonon modes  $\lambda$  with meanfreepaths ( $\Lambda_\lambda$ ) lower than  $L$  ( $k_L \propto \sum_{\Lambda_\lambda < L} C_\lambda v_\lambda \Lambda_\lambda$ ,  $C_\lambda$  is the specific heat of mode  $\lambda$ ) (since

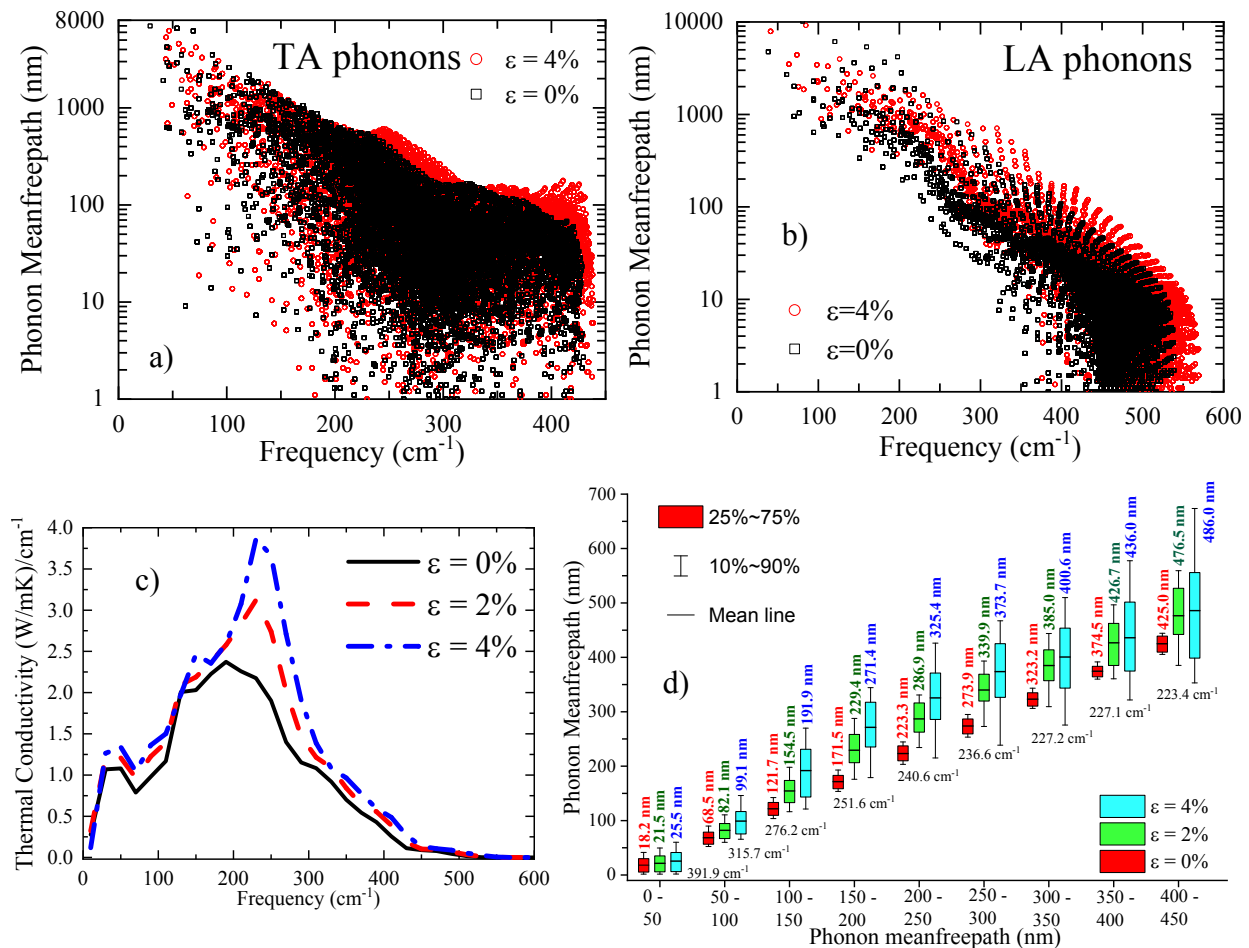


Fig. 6: Phonon meanfreepaths as a function of frequency in unstrained and strained BP of a) TA phonons and b) LA phonons. c) Spectral dependence of thermal conductivity in unstrained and strained BP and d) Change in meanfreepaths of phonons in strained BP; values above boxes represent average mean-freepath, while values below are the mean frequencies for the particular group of phonons.

higher meanfreepath phonons get scattered at the boundaries). Above increase in meanfreepaths

in nanometer regime (through a decrease in scattering which enhances phonon lifetimes  $\tau_\lambda$ ) seen in Figs. 6a and b, enhances their  $k$  contribution at nanoscale lengths (since  $k_\lambda \propto \Lambda_\lambda$ ), thus leading to enhancement in  $k$  in the nanometer regime (seen in Fig. 3b). Increase in  $\Lambda$  is seen more clearly in Fig. 6d, where we select phonons in different meanfreepath ranges in unstrained BP, such as 0 - 50 nm, 50 - 100 nm up to 400 - 450 nm, and study changes in  $\Lambda$  of the same group of phonons in strained BP. Fig. 6d shows increase in  $\Lambda$  in each group, leading to enhancement in  $k$  at all nanometer length scales presented in Fig. 3b. Above analysis clearly demonstrates that decrease in  $a + a \rightarrow o$  scattering at higher frequencies, where phonon meanfreepaths are in nanometers, leads to enhancement in  $k$  at nanometer length scales in strained BP. Presented effect of strain mediated increase in  $\Lambda$  at nanometer lengths through suppression of anharmonic scattering at higher frequencies, can be applied to enhance nanoscale  $k$  in a wide range of compound semiconductors with a phononic band gap in their vibrational spectra. Such high  $k$  semiconductors can function as efficient heat spreaders, thus improving thermal management.

Note that the effect is related to the magnitude of the phonon band gap, which determines the frequencies and therefore  $\Lambda$  at which  $a + a \rightarrow o$  scattering is dominant, thus determining the length scales at which  $\Lambda$  and  $k$  can be enhanced. This can be employed to tune  $k$  enhancement at particular nanometer length scales in different compound semiconductors through differences in phonon band gap. Biaxial strain investigated in this work, can be achieved by growth of a material on a lattice mismatched substrate<sup>31</sup>, further providing avenues for applications of outlined effect in nanoelectronics. Finally, it is noted that thermal conductivities reported in this work are computed based on the lowest order three-phonon scattering, ignoring the role of four-phonon processes, which have been shown to have minimal impact on  $k$  of BP in a recent work<sup>32</sup>.

In summary, by deriving harmonic and anharmonic interatomic force interactions, from density functional theory and using them along with an exact solution of the Boltzmann transport equation, we have provided a microscopic description of enhancement in nanoscale thermal conductivity in biaxially strained Boron Phosphide. At 200 nm, an increase in out-of-plane  $k$  of 25% is observed at 300 K, from 120.6 W/mK, for strain  $\varepsilon=0\%$ , to 150.4 W/mK, for  $\varepsilon = 4\%$ . Bulk  $k$  of 4% biaxially compressed Boron-Phosphide (BP) is also found to be enhanced to 802.5 W/mK at 300 K, almost 35.8% higher than 591 W/mK, computed for unstrained BP, and almost 5-fold the  $k$  of silicon Si. Increase in phonon band gap in strained BP, suppresses the dominant scattering channel involving scattering of acoustic phonons through absorption of other acoustic phonons in to optical phonons ( $a + a \rightarrow o$  channel), enhancing phonon lifetimes and thus material  $k$ . Furthermore,  $a + a \rightarrow o$  channel is dominant at higher frequencies; suppression of scattering at these higher frequencies, enhances phonon meanfreepaths in nanometer range, thus enhancing nanoscale  $k$ . These results have important implications for achieving efficient thermal management in nanoelectronic applications.

### Conflicts of interest

There are no conflicts of interest to declare.

### Acknowledgements

RM and JG acknowledge support from National Science Foundation CAREER award under Award No. #1847129. We also acknowledge OU Supercomputing Center for Education and Research (OSCER) for providing computing resources for this work.

## References:

1. Cahill, D. G.; Braun, P. V.; Chen, G.; Clarke, D. R.; Fan, S.; Goodson, K. E.; Keblinski, P.; King, W. P.; Mahan, G. D.; Majumdar, A.; Maris, H. J.; Phillpot, S. R.; Pop, E.; Shi, L., Nanoscale thermal transport. II. 2003–2012. *Applied Physics Reviews* **2014**, *1* (1), 011305.
2. Chen, G., Nonlocal and Nonequilibrium Heat Conduction in the Vicinity of Nanoparticles. *Journal of Heat Transfer* **1996**, *118* (3), 539-545.
3. Poudel, B.; Hao, Q.; Ma, Y.; Lan, Y.; Minnich, A.; Yu, B.; Yan, X.; Wang, D.; Muto, A.; Vashaee, D.; Chen, X.; Liu, J.; Dresselhaus, M. S.; Chen, G.; Ren, Z., High-Thermoelectric Performance of Nanostructured Bismuth Antimony Telluride Bulk Alloys. *Science* **2008**, *320* (5876), 634.
4. Zhang, H.; Hua, C.; Ding, D.; Minnich, A. J., Length Dependent Thermal Conductivity Measurements Yield Phonon Mean Free Path Spectra in Nanostructures. *Scientific Reports* **2015**, *5* (1), 9121.
5. Liu, Y.; Zhang, S.; Han, Z.; Zhao, Y., Grain-size-dependent thermal conductivity of nanocrystalline materials. *Journal of Nanoparticle Research* **2016**, *18* (10), 296.
6. de Boer, J.; Kim, D. S.; Ao, X.; Hagen, D.; Cojocaru, A.; Föll, H.; Schmidt, V., Temperature and structure size dependence of the thermal conductivity of porous silicon. *EPL (Europhysics Letters)* **2011**, *96* (1), 16001.
7. Lindsay, L.; Broido, D. A.; Reinecke, T. L., First-Principles Determination of Ultrahigh Thermal Conductivity of Boron Arsenide: A Competitor for Diamond? *Physical Review Letters* **2013**, *111* (2), 025901.
8. Lindsay, L.; Broido, D. A.; Reinecke, T. L., Phonon-isotope scattering and thermal conductivity in materials with a large isotope effect: A first-principles study. *Physical Review B* **2013**, *88* (14), 144306.
9. Lindsay, L.; Broido, D. A.; Reinecke, T. L., Thermal Conductivity and Large Isotope Effect in GaN from First Principles. *Physical Review Letters* **2012**, *109* (9), 095901.
10. Tian, F.; Song, B.; Chen, X.; Ravichandran, N. K.; Lv, Y.; Chen, K.; Sullivan, S.; Kim, J.; Zhou, Y.; Liu, T.-H.; Goni, M.; Ding, Z.; Sun, J.; Udalamatta Gamage, G. A. G.; Sun, H.; Ziyae, H.; Huyan, S.; Deng, L.; Zhou, J.; Schmidt, A. J.; Chen, S.; Chu, C.-W.; Huang, P. Y.; Broido, D.; Shi, L.; Chen, G.; Ren, Z., Unusual high thermal conductivity in boron arsenide bulk crystals. *Science* **2018**, *361* (6402), 582.
11. Chen, K.; Song, B.; Ravichandran, N. K.; Zheng, Q.; Chen, X.; Lee, H.; Sun, H.; Li, S.; Gamage, G. A.; Tian, F.; Ding, Z.; Song, Q.; Rai, A.; Wu, H.; Koirala, P.; Schmidt, A. J.; Watanabe, K.; Lv, B.; Ren, Z.; Shi, L.; Cahill, D. G.; Taniguchi, T.; Broido, D.; Chen, G., Ultrahigh thermal conductivity in isotope-enriched cubic boron nitride. *Science* **2020**, eaaz6149.
12. Broido, D. A.; Lindsay, L.; Reinecke, T. L., Ab initio study of the unusual thermal transport properties of boron arsenide and related materials. *Physical Review B* **2013**, *88* (21), 214303.
13. Garg, J.; Bonini, N.; Marzari, N., High Thermal Conductivity in Short-Period Superlattices. *Nano Letters* **2011**, *11* (12), 5135-5141.
14. Ravichandran, N. K.; Broido, D., Non-monotonic pressure dependence of the thermal conductivity of boron arsenide. *Nature Communications* **2019**, *10* (1), 827.
15. Zheng, Q.; Li, S.; Li, C.; Lv, Y.; Liu, X.; Huang, P. Y.; Broido, D. A.; Lv, B.; Cahill, D. G., High Thermal Conductivity in Isotopically Enriched Cubic Boron Phosphide. *Advanced Functional Materials* **2018**, *28* (43), 1805116.
16. Kang, J. S.; Wu, H.; Hu, Y., Thermal Properties and Phonon Spectral Characterization of Synthetic Boron Phosphide for High Thermal Conductivity Applications. *Nano Letters* **2017**, *17* (12), 7507-7514.

17. Lindsay, L.; Broido, D. A.; Carrete, J.; Mingo, N.; Reinecke, T. L., Anomalous pressure dependence of thermal conductivities of large mass ratio compounds. *Physical Review B* **2015**, *91* (12), 121202.
18. Fugallo, G.; Lazzeri, M.; Paulatto, L.; Mauri, F., Ab initio variational approach for evaluating lattice thermal conductivity. *Physical Review B* **2013**, *88* (4), 045430.
19. Paulatto, L.; Mauri, F.; Lazzeri, M., Anharmonic properties from a generalized third-order ab initio approach: Theory and applications to graphite and graphene. *Physical Review B* **2013**, *87* (21), 214303.
20. Broido, D. A.; Malorny, M.; Birner, G.; Mingo, N.; Stewart, D. A., Intrinsic lattice thermal conductivity of semiconductors from first principles. *Applied Physics Letters* **2007**, *91* (23), 231922.
21. Garg, J.; Bonini, N.; Kozinsky, B.; Marzari, N., Role of Disorder and Anharmonicity in the Thermal Conductivity of Silicon-Germanium Alloys: A First-Principles Study. *Physical Review Letters* **2011**, *106* (4), 045901.
22. Debernardi, A.; Baroni, S.; Molinari, E., Anharmonic Phonon Lifetimes in Semiconductors from Density-Functional Perturbation Theory. *Physical Review Letters* **1995**, *75* (9), 1819-1822.
23. Deinzer, G.; Birner, G.; Strauch, D., Ab initio calculation of the linewidth of various phonon modes in germanium and silicon. *Physical Review B* **2003**, *67* (14), 144304.
24. Srivastava, G. P., *Physics of Phonons*. Taylor and Francis Group: New York, 1990.
25. Giannozzi, P.; Baroni, S.; Bonini, N.; Calandra, M.; Car, R.; Cavazzoni, C.; Ceresoli, D.; Chiarotti, G. L.; Cococcioni, M.; Dabo, I.; Dal Corso, A.; de Gironcoli, S.; Fabris, S.; Fratesi, G.; Gebauer, R.; Gerstmann, U.; Gougoussis, C.; Kokalj, A.; Lazzeri, M.; Martin-Samos, L.; Marzari, N.; Mauri, F.; Mazzarello, R.; Paolini, S.; Pasquarello, A.; Paulatto, L.; Sbraccia, C.; Scandolo, S.; Sclauzero, G.; Seitsonen, A. P.; Smogunov, A.; Umari, P.; Wentzcovitch, R. M., QUANTUM ESPRESSO: a modular and open-source software project for quantum simulations of materials. *Journal of Physics: Condensed Matter* **2009**, *21* (39), 395502.
26. Monkhorst, H. J.; Pack, J. D., Special points for Brillouin-zone integrations. *Physical Review B* **1976**, *13* (12), 5188-5192.
27. Paulatto, L.; Errea, I.; Calandra, M.; Mauri, F., First-principles calculations of phonon frequencies, lifetimes, and spectral functions from weak to strong anharmonicity: The example of palladium hydrides. *Physical Review B* **2015**, *91* (5), 054304.
28. Alves, H. W. L.; Kunc, K., Lattice dynamics of boron phosphide. *Journal of Physics: Condensed Matter* **1992**, *4* (31), 6603-6612.
29. Daoud, S.; Bioud, N.; Belagraa, L.; Lebga, N., Elastic, Optoelectronic, and Thermal Properties of Boron Phosphide. *Journal of Nano and Electronic Physics* **2013**, *5*, 04061.
30. Casimir, H. B. G., Note on the conduction of heat in crystals. *Physica* **1938**, *5* (6), 495-500.
31. Clavel, M.; Goley, P.; Jain, N.; Zhu, Y.; Hudait, M. K., Strain-Engineered Biaxial Tensile Epitaxial Germanium for High-Performance Ge/InGaAs Tunnel Field-Effect Transistors. *IEEE Journal of the Electron Devices Society* **2015**, *3* (3), 184-193.
32. Ravichandran, N. K.; Broido, D., Phonon-Phonon Interactions in Strongly Bonded Solids: Selection Rules and Higher Order Processes. *arXiv:2003.08893v1* **2020**.